Proceedings of ASME Turbo Expo 2017: Turbomachinery Technical Conference and Exposition
GT 2017
June 26-30, 2017, Charlotte, NC, USA

GT2017-63857

PLASTIC EFFECTS ON HIGH CYCLE FATIGUE AT THE EDGE OF CONTACT OF TURBINE BLADE FIXTURES

C. H. Richter*, **U. Krupp, M. Zeißig**
Faculty of Engineering and Computer Science
Osnabrück University of Applied Sciences
Albrechtstr. 30, 49076 Osnabrück
Germany
Email: c.h.richter@hs-osnabrueck.de

G. Telljohann
DYNATEC GmbH
Adam-Opel-Str. 4
38112 Braunschweig
Germany

ABSTRACT
Slender turbine blades are susceptible to excitation. Resulting vibrations stress the blade's fixture to the rotor or stator. In this paper, high cycle fatigue at the edge of contact between blade and rotor/stator of such fixtures is investigated both experimentally and numerically. Plasticity in the contact zone and its effects on e. g. contact tractions, fatigue determinative quantities and fatigue itself are shown to be of considerable relevance. The accuracy of the finite element analysis is demonstrated by comparing the predicted utilizations and slip region widths with data gained from tests. For the evaluation of edge of contact fatigue, tests on simple notched specimens provide the limit data. Predictions on the utilization are made for the edge of contact of a dovetail set-up. Tests with this set-up provide the experimental fatigue limit to be compared to. The comparisons carried out show a good agreement between the experimental results and the plasticity-based calculations of the demonstrated approach.

Keywords: *turbine blade fixture, edge of contact, plastification, high cycle fatigue, fretting, experiment*

NOMENCLATURE
EOC	edge of contact
FEA	finite element analysis
A, α	material properties in Sines' criterion
a, b	material properties in Dang Van's criterion
$\mathscr{M}$	von Mises operator yielding effective stress
U	material utilization
μ	dynamic coefficient of friction
$\boldsymbol{\rho}^*$	stabilized residual stress tensor
$\boldsymbol{\sigma}$	macroscopic stress tensor
$\boldsymbol{\sigma}_{\text{meso}}$	mesoscopic stress tensor
τ_{meso}	mesoscopic shear stress

INTRODUCTION
High cycle fatigue at the edge of contact (EOC) is known to be a potential failure mode of recessive fixtures like fir-tree and dovetail roots of turbine blades as shown in Fig. 1, left. EOC cracks may grow and become critical leading to catastrophic failure. An elastic analysis usually shows a high stress gradient around the EOC crack initiation site and often demonstrates crack arrest as a consequence of the high gradient. This arrest mechanism is less prevailing if plasticity flattens out the stress field, Fig. 1, right. A benefit from plasticity is a lowered stress level. For various applications in mechanical engineering, EOC cracks are known to grow. Although EOC fatigue is a severe failure mode, its analysis is not part of the standard design process. Sole structural optimization of the nearby notch, neglecting analysis of the EOC, may lead to that failure mode becoming the limiting factor of design without recognition. Therefore, it is important to design against this failure mode. However, fatigue tests including contact to acquire design limits are usually costly.

In the past decades, EOC fatigue or fretting fatigue has been studied based on different fixture types experimentally and ana-

*Address all correspondence to this author.

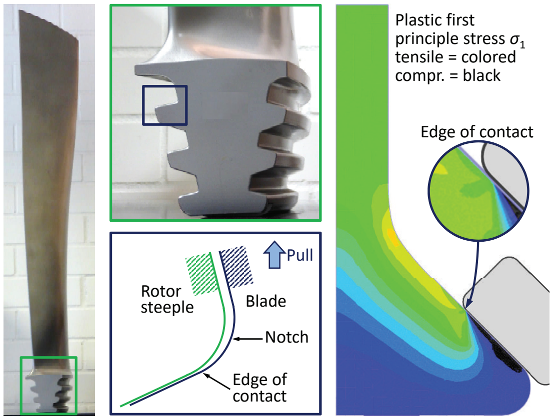

FIGURE 1. LEFT: FIR-TREE ROOT OF A TURBINE BLADE, ZOOM ON EDGE OF CONTACT. RIGHT: REPRESENTATIVE STRESS FIELD.

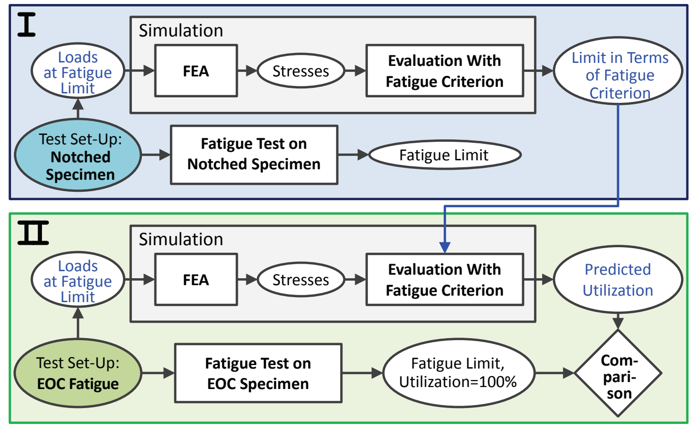

FIGURE 2. METHODOLOGY EMPLOYED FOR EOC FATIGUE.

lytically, while the material has often been considered in its elastic range. A solely elastic approach, however, might be insufficient as the application of an overload prior to service, being typical for turbine applications, leads to local plastification in the range of the EOC. This gives rise to remaining indentations on the contact surfaces and to residual stresses. In consequence, this leads to a load redistribution of both, mean stress due to centrifugal forces and dynamic stress due to vibration. Further sources of plastification, like shot peening, are in practice as well, demanding respective consideration.

In recent times plasticity has gained attention as a factor in EOC fatigue. For example [1] studies severe EOC loading conditions leading to cyclic plasticity on the macroscopic scale. Different plastic material models are evaluated. A comparison between elastic and plastic analyses is carried out, highlighting the role of plasticity in EOC fatigue.

In [2] a plastic finite element analysis (FEA) is evaluated by combining the method of critical distances and the strain range method. This approach displays a failure criterion applicable to EOC fatigue involving plastic deformation.

In the present paper, plastic effects on high cycle fatigue at the EOC are examined based on a dovetail set-up that is similar in materials, geometry and loading to a turbine blade root fixture. The assumed operation includes an initial overload leading to distinct plastification. Loads are defined at levels as found in blade applications. Experiments on this set-up serve to validate the numerical simulation that refers to design limits gained with tests on sharply notched round specimens.

APPROACH AND METHODOLOGY

The applied methodology consists of two parts as shown in Fig. 2, each combining experiments and numerical simulations. The simulation process is the same in both parts. In Part I, the load at the fatigue limit of a simple specimen is employed to identify material limits. In Part II, these limits are applied to the simulation of the EOC set-up. Again, the experimentally gained load at the fatigue limit is used. Therefore, this simulation ought to show a utilization of 100% and hence allows the assessment of the approach.

Part I. A notched round specimen is investigated as it provides an adequate representation of the elastically calculated stress level and stress gradient as met at an EOC. For this specimen the fatigue limits at different mean loads are determined by test. The corresponding static and dynamic loads are subsequently input to a FEA of this experimental set-up yielding the stress fields. These are evaluated using a fatigue criterion in order to obtain its values right at the fatigue limits. In Part II, these are applied as the limits for the assessment of the EOC.

Part II. The EOC analysis is aligned with Part I. In other terms, the EOC set-up undergoes the same simulation process at its experimentally determined fatigue limit as carried out in the previous part. The test set-up is used to determine the fatigue strength under contact conditions. The experimental result provides the fatigue limit and the respective loads. The test rig is calculated using FEA to determine the occurring stresses at the fatigue limit. Their evaluation, applying the fatigue criterion and its associated limits as obtained in Part I, provides a predicted utilization at the EOC.

Finally, the experimental utilization at the EOC, by its definition 100%, and the predicted utilization are compared allowing a judgment of the approach consisting of the simulation and the method of limit data determination.

Scheme. The outlined procedure is carried out independently based on elastic as well as plastic material FEA. For the fatigue evaluation the criteria according to Sines [3] and Dang Van [4–6] are applied on each of the FEA. A basic comparison

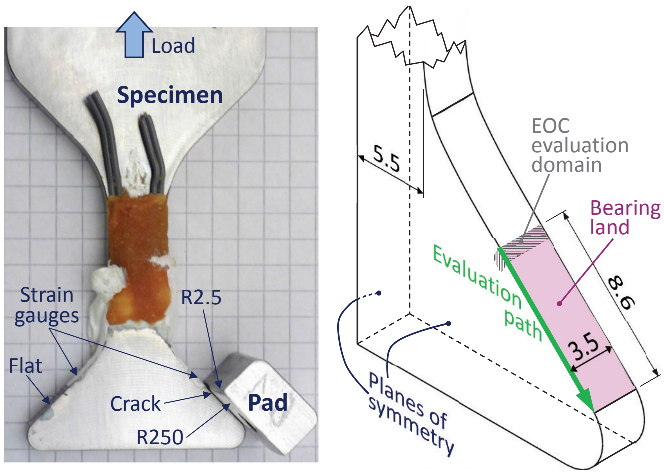

FIGURE 3. DOVETAIL SPECIMEN AND PAD.

of these criteria among others can be found in [7]. The results of all four computations are judged separately and compared to each other.

DOVETAIL SET-UP, TEST PROCEDURE AND RESULTS

Design. A dovetail set-up has been chosen for the experiments on EOC fatigue. Because of its statical determinacy – in contrast to fir-tree roots – it does not show as much sensitivity towards geometric deviations. Figure 3, left, shows a photograph of a specimen with instrumentation and a pad. On the right, a quarter of the specimen with some dimensions, the evaluation domain and the evaluation path referenced later on is shown. As is typical for this kind of recessive arrangement, the relative motion at the EOC due to vibration is in the range of just up to a few µm. The specimen is made of X5CrNiCuNb17-4PH and the pads consist of 26NiCrMoV14-5. Their yield limits are in the same order of magnitude of around 800 MPa. The dynamic coefficient of friction μ for this material pairing has been measured to be around 0.8 which is used throughout the analyses.

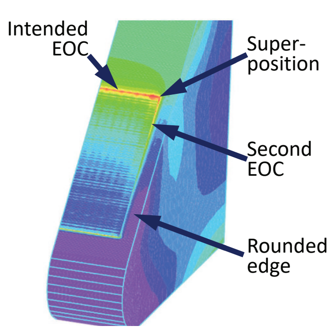

FIGURE 4. JOINING OF TWO EOC STRESSES LEADING TO POTENTIALLY UNCONTROLLABLE SITUATION DURING TEST.

The EOC test has been designed by comprehensive FEA. The initial design assumed flat contact surfaces on specimen and pad. In the course of the analyses, it has been found that in the case of a rounded face-side edge along the bearing land, a second EOC is created, Fig. 4. This is due to the stiffness present in the material below the rounding (and free of any contact). This second EOC meets the intended EOC stress concentration at the corner of the bearing land where they add up to a maximum.

Though the second EOC is comparably moderate, the resulting situation may not be well controllable during the experiment as the life-leading location appears to be right at the location of superposition. This gains in importance in view of potentially present effects like parasitic bending.

Dropping the rounding, on the other side, may lead to crack starters at the sharp corner of the edge which may distort the test result. To avoid both these situations it has been decided to employ a Hertzian contact with a small stress gradient in thickness direction. This has been achieved by shaping the pads with a radius of 250 mm in thickness direction of the specimen. The pad's radius along the intended EOC is 2.5 mm. This way, it can be ensured that the life-leading location is situated on the symmetry plane.

Test And Results. Tests have been run up to 10^7 cycles to identify the fatigue limit and its corresponding loads. The load history of the test is graphed in Fig. 5. It shows an initial overload of 150.6% with subsequent drop to a mean load of 100% (net neck stress of 465 MPa, 7 mm x 11 mm) which is kept constant for the remainder of the test. Following the one-time overload, the load is not entirely released in order to prevent additional sources of variation such as back-plastification. The outcome of the experiments is an average fatigue limit, i. e. a dynamic stress amplitude, in terms of load representing 19.3% of the static load. The obtained standard deviation amounts to 7% of the fatigue limit. Self-evidently, the experimental utilization at the fatigue limit is 100% setting the goal for the simulations.

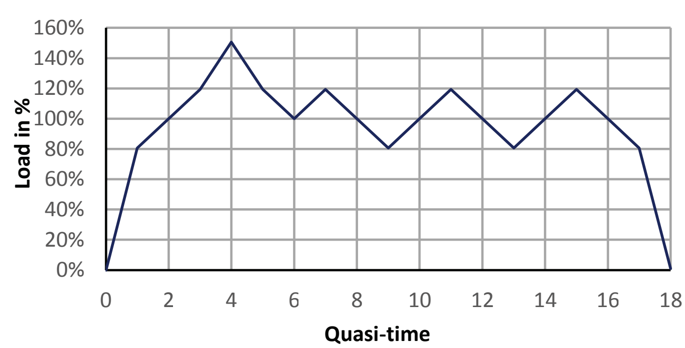

FIGURE 5. LOAD FUNCTION EMPLOYED IN TESTS AND FEA, AMPLITUDE IS EXEMPLARY.

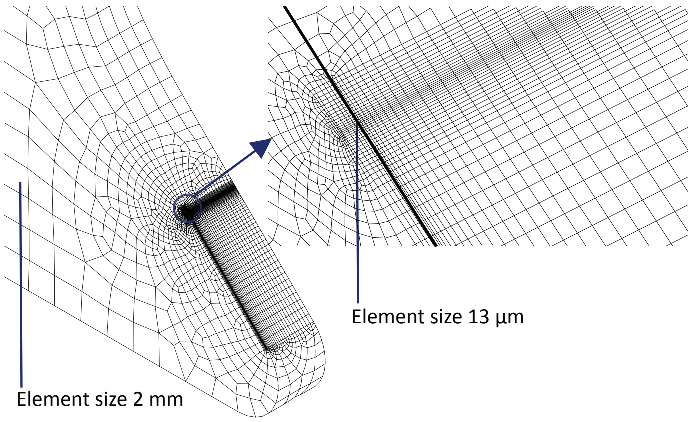

FIGURE 6. MESH OF DOVETAIL SPECIMEN.

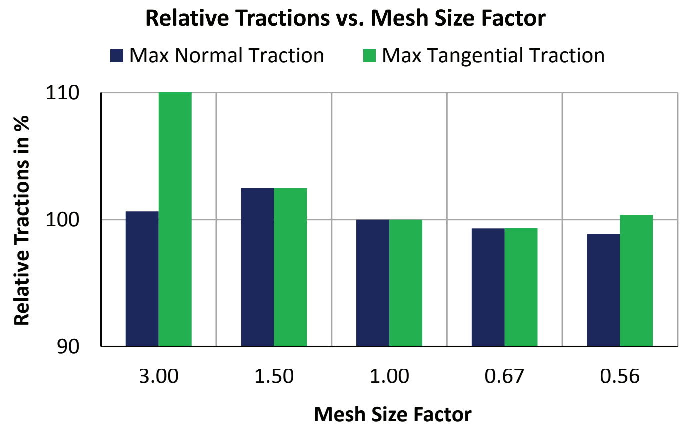

FIGURE 7. CONVERGENCE DIAGRAM OF NORMALIZED TRACTIONS VS. MESH SIZE FACTOR.

FINITE ELEMENT MODEL OF DOVETAIL SET-UP

Modeled Domain. The underlying problem of Hertzian contact with a two-dimensional curvature of the surface pairing does not allow to be approximated by a 2D model as the field gradients in thickness direction are too large in this case. Therefore, a 3D model has to be set up. ADINA [8] is used for all FEA calculations. To account for potential rotational motion of the pads while loading, their holding fixture is included in the model beside the specimen and pads. Due to its double symmetry only a quarter of the set-up is modeled.

Discretization. The contact surfaces are discretized with rectangular, linear contact segments and the solid bodies employ quadratic 20-node elements. The hexahedral volumes of 0.25 mm thickness below the contact surfaces are filled with solid, rectangular elements using rule-based meshing. Figure 6 shows the mesh of the specimen with some element sizes.

Focus of the model is to produce reliable results in the EOC domain. Contact demands small elements to resolve the traction, stress and slip field. At the location of crack initiation on the symmetry plane of the specimen at the EOC, the edge length of the quadratic elements is 13 µm. The linear contact segments show half that length. Element sizes are graded away from that point in all three spatial directions. Further coarsening of the mesh is applied moving away from the surface layer using a free-form hexahedral mesh.

Material And Friction Model. For the plastic simulations, the Mróz material model [9] is employed for the specimen and the pad. It reflects kinematic hardening only, however, because of the chosen load history which prevents back-plastification, this is of minor relevance. Static flow curves are applied, as the material is unlikely to reach the cyclic flow curve during the test in view of the applied amplitudes. The Coulomb friction model is employed. Heating due to vibration is neglected. Local heating occurs at the tips of surface asperities spreading out into the fatigue relevant zone of the base metal. Given the very small magnitude of relative motion, the impact of thermal effects is expected to be insignificant.

Convergence Study. Five different mesh size constellations have been examined for convergence. Figure 7 shows the maximum normal and tangential tractions against the mesh size factor, normalized by their values obtained with mesh size factor 1. Under evaluation of further parameters and with a view to convergence and computational effort, the mesh of size factor 1 has been chosen.

COMPARISON OF ELASTIC AND PLASTIC FEA RESULTS OF DOVETAIL SPECIMEN

Plastic yielding of the material influences the behavior of the contacting bodies. Observations on various quantities affected by yielding are presented in comparison with the elastic behavior in the following. The underlying load amplitude corresponds to the experimentally determined fatigue limit.

Remaining Indentation of Surfaces. The remaining change in contact surface shape of the mating bodies due to plastic yielding is examined. To analyze this deformation, the contact gap field at zero load is considered. This takes place before and after the static and dynamic load application, $t = 0$ and $t = 18$. The difference between these two is the remaining change in gap. It reflects yielding of both sides, the specimen and the pads. Its distribution on the upper 3 mm (of 8.6 mm) of the bearing land at the EOC is shown in Fig. 8. The amount of maximum remaining deformation is in the same order of magnitude as the typical manufacturing tolerance of a dovetail or fir-tree root. Because the test set-up including its load history is similar to blade arrangements and their loading, this statement can be transferred to blade applications in general. As a result of the permanent deformation of the bearing flanks a load re-distribution takes place. With regard

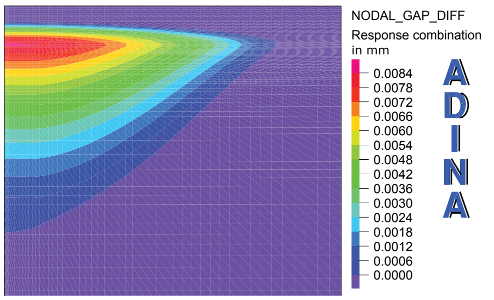

FIGURE 8. PLASTIC CHANGE IN LOAD-FREE CONTACT GAP DUE TO LOADING HISTORY FROM T=0 TO T=18.

to the comparable magnitudes of deformation and tolerance this appears to be relevant for fatigue analyses. Therefore, it seems to be advisable to include this effect in analyses by applying plastic material models for contacting parts.

Contact Tractions. Due to a plastically modified contact match of the bearing lands, the transmission of the contact tractions is changed. Figure 9 shows the normal tractions at instants of maximum ($t = 15$), mean ($t = 14$, $t = 16$) and minimum ($t = 13$, $t = 17$) load for the elastic FEA results. The same information is shown for the plastic case in Fig. 10. The point to be observed is the relative distribution of normal traction. In the plastic case, wider ranges are highly stressed though on a lower level than in the elastic case. This is caused by plastic flow itself and the resulting load re-distribution.

The local normal traction gives the limit for local sticking and for the tangential tractions of mating surfaces, thus it influences sliding distances. The images of the distribution of the tangential traction (not reproduced here) appear basically similar to the images of the normal traction.

Motion of Traction Peaks. The tangential traction along the evaluation path according to Fig. 3 is shown for some instants of the last calculated and stabilized cycle in Fig. 11 for the elastic FEA and in Fig. 13 for the plastic FEA. The tangential tractions at the mean and minimum instants of a cycle are virtually identical, aside of deviations in the range of the EOC which are due to frictional hysteresis.

The difference between the upper- and lower-most traction during a cycle is considered as it influences fatigue. Varying the specimen load, i. e. walking through the cycle, shifts the graph of traction vertically but also, and probably even more relevant, the peaks and valleys move location-wise. The latter effect takes place at the EOC because of opening and closing of the contact and because relative slip of the mating parts takes place there (however, relative motion is small in the application presented here). In consequence, the difference between upper and lower traction envelope shows large amplitudes.

Locations overrun by the moving peak during a cycle experience large variations in stressing, in other terms they experience large stress amplitudes. This is a major effect in EOC fatigue or fretting fatigue. Similar is not observed at notches in absence of contact.

The valleys in the tangential tractions along the path could not be finally explained. An investigation revealed, that they form during the overload. Since they appear in elastic and plastic FEA, they may be related to local slip producing local unloading which settles during cycling. Very similar valleys develop with notedly different FEA models. Another possible explanation not to be excluded may still be seen in local numerical deviations.

The normal tractions do not show moving peaks. Graphs at times of equal load do not show relevant deviation as observed for the tangential tractions. This is due to the negligible relative slip.

Fatigue Determinative Quantities. Looking at the fatigue criterion by Sines its determinative factors are the octahedral shear stress amplitude, in the following applied in the form

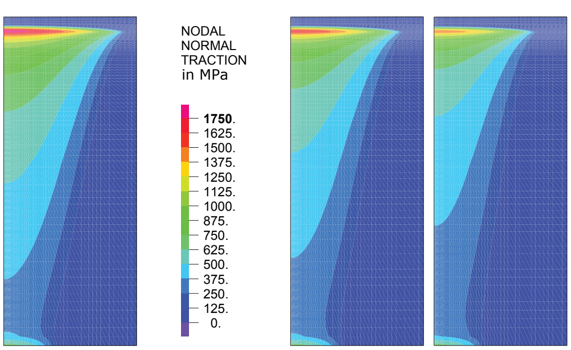

FIGURE 9. SEQUENCE OF ELASTIC NORMAL TRACTIONS ON BEARING LAND, CF. FIG. 3, DURING HALF A LOAD CYCLE.

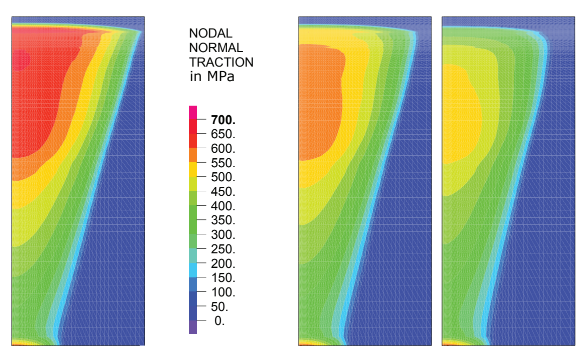

FIGURE 10. SEQUENCE OF PLASTIC NORMAL TRACTIONS ON BEARING LAND, CF. FIG. 3, DURING HALF A LOAD CYCLE.

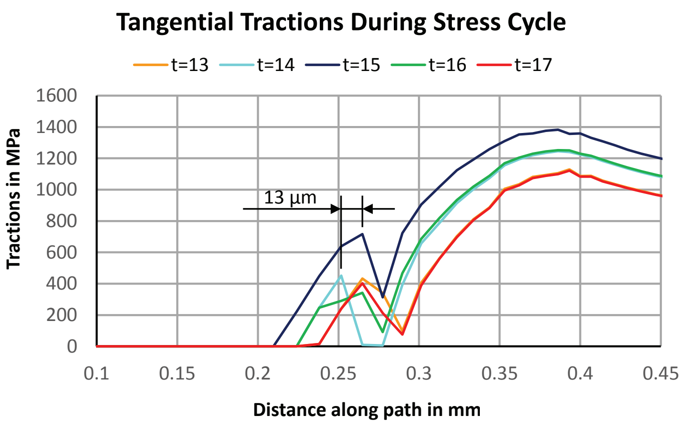

FIGURE 11. ELASTIC TANGENTIAL TRACTIONS DURING LOAD CYCLE.

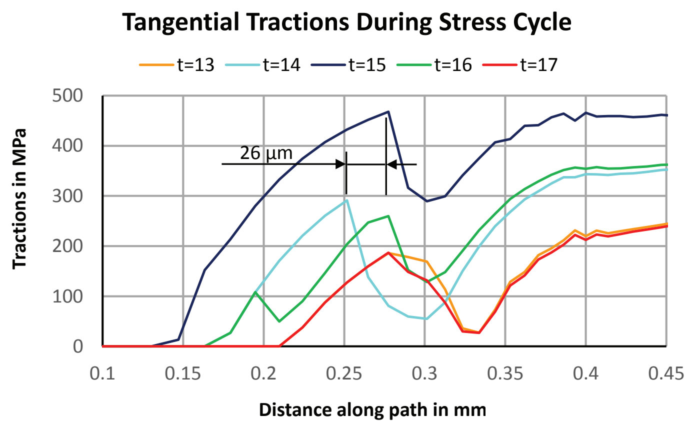

FIGURE 13. PLASTIC TANGENTIAL TRACTIONS DURING LOAD CYCLE.

of the von Mises stress amplitude, and the hydrostatic stress. The latter one is also input to the Dang Van criterion. Figure 12 and Fig. 14 show these quantities along the evaluation path obtained for elastic and plastic FEA, respectively, for the last calculated cycle. The amplitudes inherently reflect the aforementioned motion of the peaks.

As can be seen in Fig. 12 for the elastic case the peaks of the hydrostatic stress and stress amplitude appear at the same location. This is different for the plastic calculation, Fig. 14. There, the amplitude itself appears on a lower level and more wide-spread around its maximum. Aside from that location the amplitudes are approximately equal. At the predicted locations of crack initiation, around 0.2 mm as displayed later, the stress gradient is virtually insignificant, which also holds for all other spatial directions. Carrying out the FEA with plastic material models covers the macroscopic support effect in fatigue.

FATIGUE EVALUATION

This section describes the fatigue criteria employed for the evaluation of the FEA results. They are implemented into GNU Octave [10] for an automated routine. Beyond that, the determination of the design limits in terms of the mentioned criteria is displayed.

Sines Criterion. The Sines criterion [3] is based on the assumption that the dynamic shear stresses propel dislocations which accumulate and a micro-crack is formed. The octahedral shear stress serves as measure of the shear. A catalyst in this process of fatigue accumulation is the normal stress on the plane of octahedral shear stress amplitude. Tension eases the motion of dislocations. The criterion does not account for potentially varying shear stress directions which may develop under non-proportional loading.

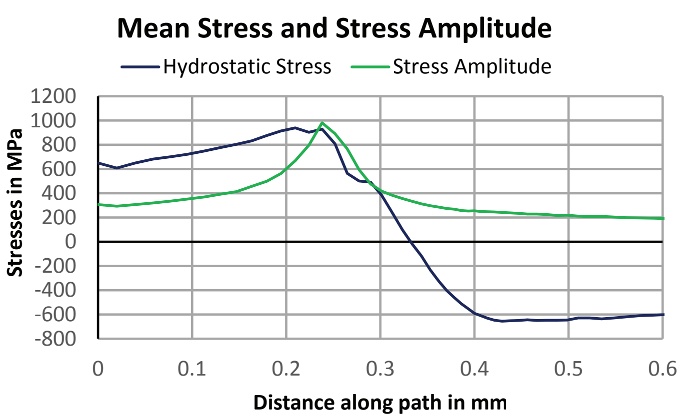

FIGURE 12. ELASTIC MEAN STRESS IN TERMS OF HYDROSTATIC STRESS AND VON MISES STRESS AMPLITUDE OF LOAD CYCLE.

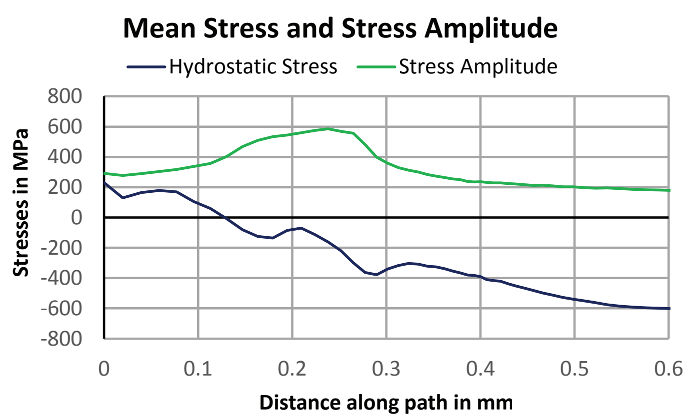

FIGURE 14. PLASTIC MEAN STRESS IN TERMS OF HYDROSTATIC STRESS AND VON MISES STRESS AMPLITUDE OF LOAD CYCLE.

An inequality equivalent to Sines' original formulation reads

$$\sigma_{\text{Mises ampl}} \leq B - \beta \cdot \sigma_{\text{h}} \tag{1}$$

It incorporates the von Mises stress amplitude $\sigma_{\text{Mises ampl}}$, being proportional to the octahedral shear stress amplitude, and the mean hydrostatic stress σ_{h}. B and β are parameters characterizing the endurance of the material. Fatigue is predicted to occur if the von Mises stress amplitude $\sigma_{\text{Mises ampl}}$ exceeds the limit line $B - \beta \cdot \sigma_{\text{h}}$.

The von Mises stress amplitude is calculated as

$$\sigma_{\text{Mises ampl}} = \frac{1}{2}\mathscr{M}\left[\boldsymbol{\sigma}(t^{\text{u}}) - \boldsymbol{\sigma}(t^{\text{l}})\right] \tag{2}$$

with $\mathscr{M}[\cdot]$ being the von Mises operator yielding the effective stress of an input stress tensor. t^{u} and t^{l} are the instants of upper and lower load, respectively. Sometimes this equation is seen with reversed order, i. e. von Mises operator and difference calculation are exchanged. However, that form does not reflect the driving force of fatigue as adequately as the equation above because e. g. constant von Mises stress state histories, indicating infinite life, may well have large variations in shear stress, hence leading to fatigue.

Dang Van Criterion. The Dang Van criterion [4] is based on the assumption that local plastic deformation at the grain level – or mesoscopic level – causes fatigue. Furthermore, elastic shakedown at the macroscopic level is assumed. Opposite to Sines' criterion, which is based on characteristics of the cycle, Dang Van's criterion is applied to a full cycle time history-wise. Its time-parameterized path is checked for momentary exceedance of a limit curve which would indicate fatigue. It reads

$$\tau_{\text{meso}}(t) \leq b - a \cdot \sigma_{\text{meso h}}(t) \tag{3}$$

with the mesoscopic shear stress τ_{meso}, the mesoscopic hydrostatic stress $\sigma_{\text{meso h}}$ and the material parameters a and b.

The macroscopic and mesoscopic stress tensors are related via the stabilized residual stress tensor $\boldsymbol{\rho}^*$ on the mesoscopic level. This tensor is the center of a six dimensional minimum hypersphere embracing the entire stress path during a cycle of the macroscopic stress $\boldsymbol{\sigma}(t)$.

$$\boldsymbol{\sigma}_{\text{meso}}(t) = \boldsymbol{\sigma}(t) - \text{dev}(\boldsymbol{\rho}^*) \tag{4}$$

Based on that, the mesoscopic shear stress τ_{meso} is computed using Tresca maximum shear stress theory on the principal stresses σ_i of $\boldsymbol{\sigma}_{\text{meso}}(t)$.

$$\tau_{\text{meso}}(t) = \frac{1}{2}[\sigma_{\text{meso 1}}(t) - \sigma_{\text{meso 3}}(t)] \tag{5}$$

The mesoscopic hydrostatic stress is identical to the macroscopic hydrostatic stress since $\boldsymbol{\rho}^*$ enters Eq. (4) with its deviatoric part only. Thus, it can be formulated as

$$\sigma_{\text{meso h}}(t) = \frac{1}{3}\text{tr}[\boldsymbol{\sigma}(t)] \tag{6}$$

Equation (3) predicts fatigue if the mesoscopic shear stress path in a $\tau_{\text{meso}}(t)$ versus $\sigma_{\text{h}}(t)$ diagram exceeds the limit curve $b - a \cdot \sigma_{\text{meso h}}$ in any point.

In this form the criterion is widely applied to elastic as well as to elastically modeled problems that macroscopically leave the elastic range but maintain elastic shakedown. Beside an elastic model, here it is applied to a model that includes macroscopic yielding and elastic shakedown. This approach is expected to yield a more realistic residual stress tensor $\boldsymbol{\rho}^*$ and hydrostatic stress σ_{h}. Applying the Dang Van criterion to plastic FEA, the determination of the design limits by round specimen is also based on plastic FEA, following the aligned branches I and II in Fig. 2.

Design Limits by Round Specimen. Following the methodology previously outlined, the described endurance criteria are applied to fatigue test results of a round specimen to identify the design limits for the EOC evaluation.

Specimen Design. The suggested round specimen is a simple turned part, hence facilitating cost-effective fatigue tests for Part I of the methodology. Its application requires a stressing resembling that found at the EOC. This stressing is controlled by two parameters. Firstly the peak stress itself which is adjusted by the load and secondly the stress gradient at the peak stress location. The latter one has been determined based on elastic FEA of the dovetail set-up and is transferred to the round specimen on an elastic basis. The analyses result in a sharply notched specimen with notch radius of 0.1 mm. The inclusion of the stress gradient in the limit-defining tests renders an explicit quantification of micro-support superfluous.

Mean Stress Influence. In order to grasp the influence of the mean load on the endurable vibration amplitude, two load cases, A and B, have been defined. These supply the endurance limit at two different hydrostatic stresses. Table 1 displays the respective static and dynamic loads. Both, the initial overload and the imposed load history are aligned with the EOC test, Fig. 5.

Fatigue Test Evaluation. For the fatigue test evaluation of the notched specimens, the identified dynamic loads at the fatigue limit are input to axisymmetric elastic and plastic FEA of the test set-up. Afterwards, the calculated stresses of the two load cases and of both material cases are evaluated with each of the fatigue criteria. This allows to determine the design limit in terms of the particular criterion.

The application of the Sines criterion on the elastic and plastic FEA results for each load case, A and B, is shown in

TABLE 1. LOADS OF THE ROUND SPECIMEN.

Load case	Overload	Mean load	Fatigue limit
A	150.6%	100.0%	27.7%
B	150.6%	123.5%	23.6%

Fig. 15. Each dot in that graph represents a location in the neck of the specimen. The most critical nodes, defining the limit curve (black) are determined as the nodes with maximum stress amplitudes. They are located on the surface.

The plot of the Dang Van evaluation for the elastic and plastic FEA results is shown in Fig. 16. It shows the time-parameterized graphs during the last calculated cycle of both load cases, A and B, for the critical locations, which are also on the surface. The limit curve is defined by the points on the upper right of the V-shaped graphs corresponding to a time instant of maximum load.

The maximum von Mises stress amplitudes are found to be virtually the same for the elastic and plastic results. They are accompanied by different mean stresses due to plastification effects. The same holds for the mesoscopic shear stresses. In contrast to the behavior of notches free of contact, the amplitudes at the EOC are different for the elastic and plastic case as shown in Fig. 12 and Fig. 14. Hence, the reason for that appears to be related to contact.

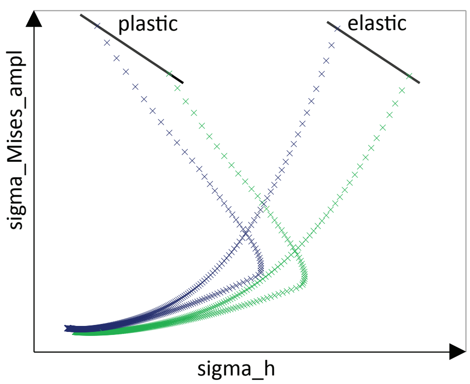

FIGURE 15. ELASTIC AND PLASTIC LIMIT CURVES (BLACK) FOR THE SINES CRITERION DETERMINED FROM LOAD CASES A (BLUE) AND B (GREEN).

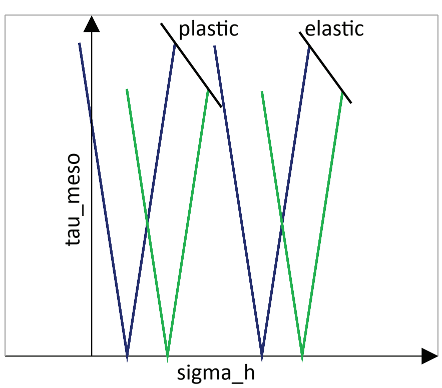

FIGURE 16. ELASTIC AND PLASTIC LIMIT CURVES (BLACK) FOR THE DANG VAN CRITERION DETERMINED FROM LOAD CASES A (BLUE) AND B (GREEN).

PREDICTIONS AND DISCUSSION FOR DOVETAIL SET-UP

In this section, the round specimen-based limit curves are applied to the FEA results at the EOC. Following the alignment of the methodology in Part I and II, Fig. 2, the results to be evaluated and the limit curves are paired according to equal material models. For illustration purposes, this evaluation is confined to locations of the EOC evaluation domain and evaluation path on the symmetry plane as given in Fig. 3. The critical point of crack initiation is contained.

Sines. The Sines results for the elastic and plastic FEA are given in Fig. 17 and Fig. 19, respectively. The grid widths in mentioned diagrams are separately equal in each direction to allow comparison.

The elastic results show significantly higher mean stresses and von Mises amplitudes than the plastic results. Opposite to the plastic case, the elastic results considerably exceed the endurance criterion.

Dang Van. Similar observations can be made for the results of the Dang Van evaluation. Each time-parameterized graph of mesoscopic shear stress against hydrostatic stress shown in Fig. 18 for the elastic case and Fig. 20 for the plastic case corresponds to one node during the last calculated cycle. The grid widths in mentioned diagrams are separately equal in each direction. Again, the stresses are smaller for the plastic results. In the elastic case the limit curve is clearly exceeded, while in the plastic case the limit curve is not reached.

Some of the graphs do not show a clear V-shape. These belong to locations close to the zone where fluctuations in contact status take place during the cycle. This reflects the zone of partial slip.

Comparison of Utilizations. The utilization is defined as the quotient of the occurring dynamic stress, left sides in Eqs. (1) and (3), and the associated limit, right sides of said equations. The predicted and experimental utilizations of the dovetail

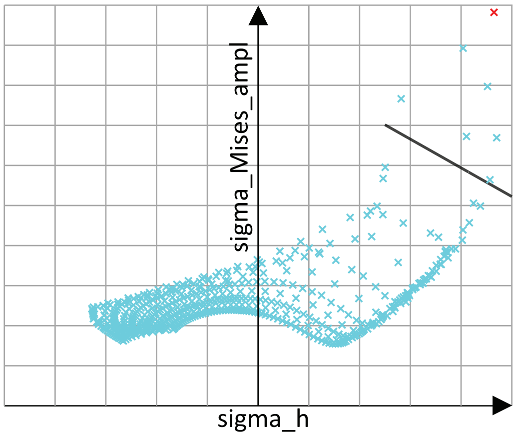

FIGURE 17. SINES EVALUATION OF ELASTIC FEA.

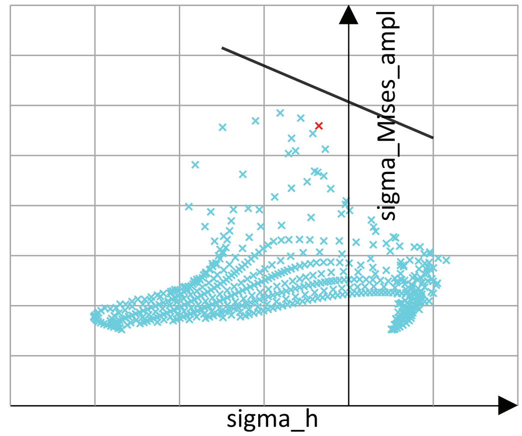

FIGURE 19. SINES EVALUATION OF PLASTIC FEA.

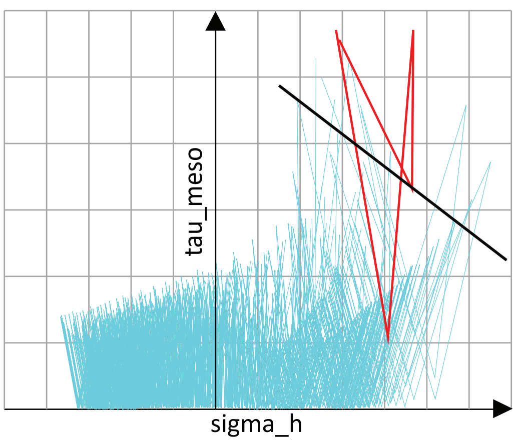

FIGURE 18. DANG VAN EVALUATION OF ELASTIC FEA.

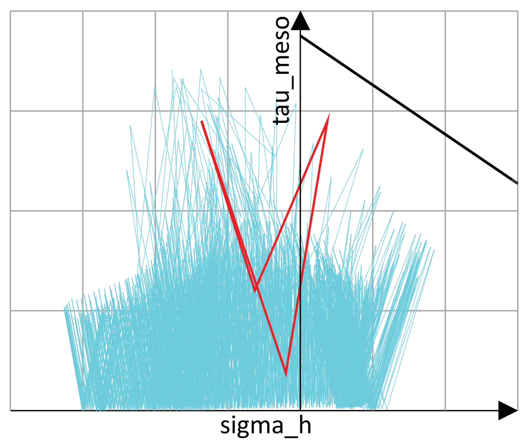

FIGURE 20. DANG VAN EVALUATION OF PLASTIC FEA.

fatigue test are compared for the elastic and plastic calculations and for both criteria. Fatigue contributions from the one-time overload are negligibly small and thus not considered.

The elastic- and plastic-based utilizations in the EOC evaluation domain are given in Fig. 21 for the Sines criterion and in Fig. 22 for the Dang Van criterion. The results obtained correspond quite well considering each material case individually. In all four cases, the most critical nodes are located on the surface and symmetry plane.

A summary of the utilizations for both criteria in the elastic and plastic case is given in Tab. 2. As stated in Section *Approach and Methodology*, the target value is 100%. There is a considerable difference between the elastic- and plastic-based utilizations in both criteria. As seen before, the elastic results significantly exceed the criteria limits with utilizations of 179% for Sines and 173% for Dang Van. The values of the plastic evaluations are 89%, Sines, and 85%, Dang Van.

Slip Region And Crack Initiation Location. The utilization along the evaluation path is displayed together with the contact status during the last calculated cycle in Fig. 23, elastic, and Fig. 24, plastic. The contact statuses are plotted against location as horizontal lines whose extents mark the location of their validity. The overlap of these lines indicates a local change in status during a load cycle. For the elastic case, identical crack initiation locations are predicted by the Sines and Dang Van evaluations. The critical locations calculated for the plastic case are different by 45 µm.

The calculated maximum utilizations, hence the critical nodes, are situated in the slip region. Slip on its own, is not the cause for potential fatigue but the resulting tractions and therefore stresses. As said before, the motion of the stress peaks at the EOC, related to the opening and closing of the contact at that location, imposes high stress amplitudes. In this way, the observed fretting corrosion is to be understood as an indicator

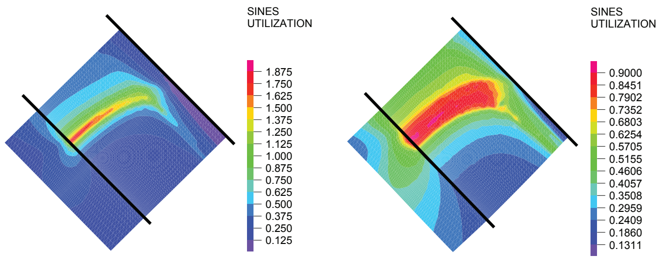

FIGURE 21. LOCAL UTILIZATION IN THE EOC EVALUATION DOMAIN, CF. FIG. 3, ACCORDING TO SINES, LEFT: ELASTIC, RIGHT: PLASTIC.

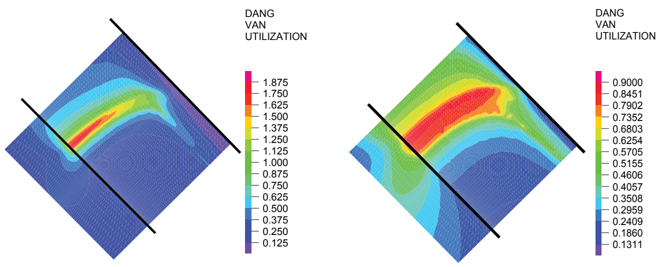

FIGURE 22. LOCAL UTILIZATION IN THE EOC EVALUATION DOMAIN, CF. FIG. 3, ACCORDING TO DANG VAN, LEFT: ELASTIC, RIGHT: PLASTIC.

for stress. Slip might gain further influence by that it roughens the surface thus making it susceptible to fatigue and raising the coefficient of friction. The utilization is significantly lower in the sticking area due to compressive hydrostatic stresses that lead to higher admissible amplitudes, and smaller occurring amplitudes.

According to the plastic analysis the critical location experiences a moderate compressive hydrostatic mean stress, Fig. 14. Looking at the cyclic mesoscopic shear stress path $\tau_{\text{meso}}(t)$, red line in Fig. 20, the critical instant and its close surroundings feature tensile hydrostatic stresses while a large portion of the cycle takes place under compression. In short, the critical location is observed in the transition from compressive to tensile hydrostatic mean stress.

TABLE 2. MAXIMUM UTILIZATIONS, TARGET SET BY EXPERIMENT: 100%.

	Elastic	Plastic
Sines	179%	89%
Dang Van	173%	85%

The width of the slip region at the location of potential fatigue failure is represented by the length of the green lines in Fig. 23 and Fig. 24. Based on elastic FEA 40 µm are obtained, in the plastic case this amounts to 145 µm. An evaluation of tested uncracked specimens for the slip region width by measuring the fretting corrosion strip in the vicinity of the potential failure location reveals values around 140 µm as shown in the right of Fig. 25. Moreover, a comparison of the sideways slip regions is shown there in the left and middle image referring to FEA and test, respectively. Both show an inclined path along the bearing land.

It was not possible to measure the location of the crack initiation site on the cracked specimens with sufficient accuracy as these suffered from secondary damage created while running beyond initiation.

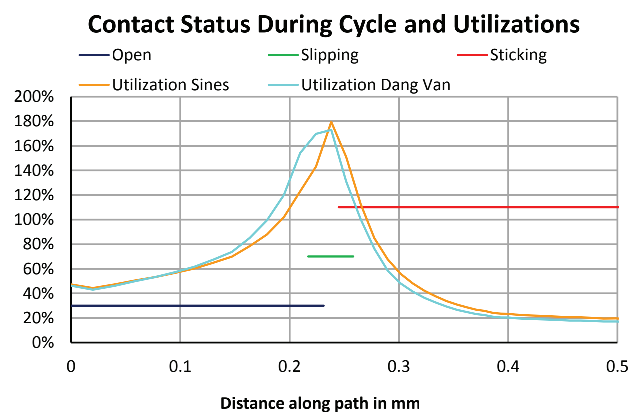

FIGURE 23. CONTACT STATUS DURING CYCLE AND UTILIZATIONS, SINES AND DANG VAN, ALONG THE EVALUATION PATH, BASED ON ELASTIC FEA.

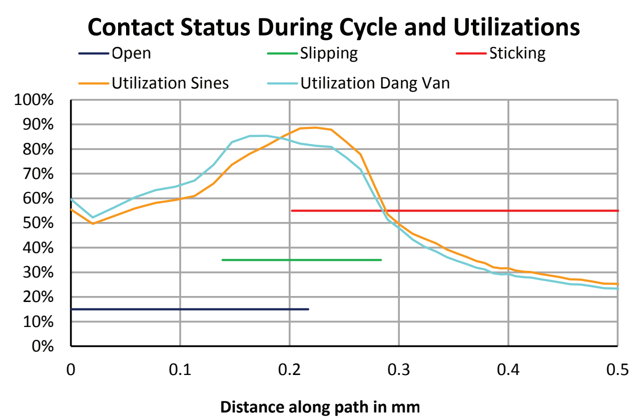

FIGURE 24. CONTACT STATUS DURING CYCLE AND UTILIZATIONS, SINES AND DANG VAN, ALONG THE EVALUATION PATH, BASED ON PLASTIC FEA.

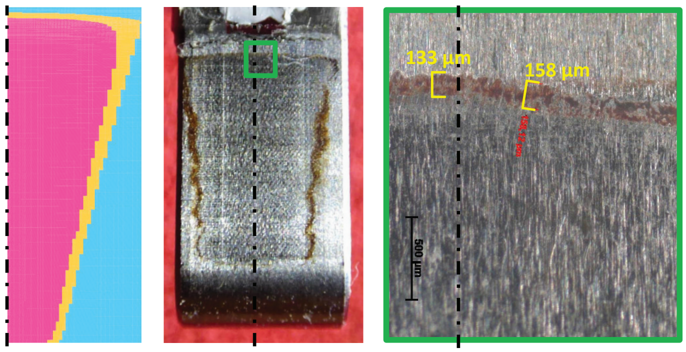

FIGURE 25. LEFT: SLIDING REGION VIA FEA (ORANGE), MIDDLE: PHOTOGRAPH OF BEARING LAND OF AN UNCRACKED SPECIMEN SHOWING FRETTING CORROSION INDICATING THE SLIP REGION, RIGHT: ZOOM ON EOC WITH DIMENSIONS OF CORROSION WIDTH.

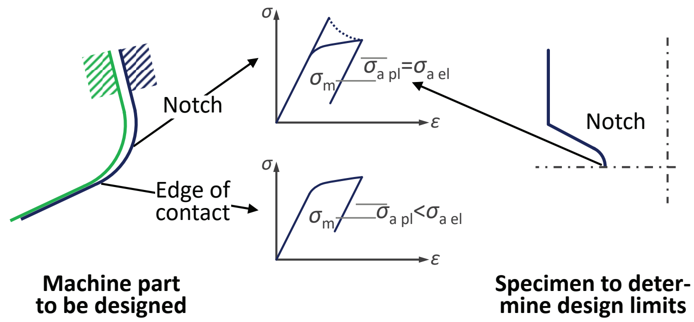

FIGURE 26. ELASTIC AND PLASTIC RESPONSE AT NOTCH AND EOC, RELATION TO NOTCHED SPECIMEN.

Transfer to Design Application. There are various sectors in mechanical engineering that have to deal with EOC fatigue [11]. Depending on the risk connected with the failure of an affected component an individual validation by contact test may be sensible.

Once validated, the scheme may be applied in component analysis. The 'Test Set-Up: EOC Fatigue' in Part II of the methodology, Fig. 2, has to be replaced by the component. Expensive component tests involving contact can be omitted, only the simulation needs to be carried out. Part I is required to gain design limits for the actual material.

Elastic Versus Plastic Approach. The reason for the large difference in the prediction of elastic and plastic utilizations is summarized in the following. For demonstration purposes, some machine part having a notch (free of contact) and an EOC zone is considered, Fig. 26, left.

The analysis of that machine part's notch is considered first. Static loads are assumed to cause plastification at the notch root. A vibratory load stresses it in elastic shakedown. The elastic and plastic analyses yield similar stress amplitudes as can be made plausible by looking at the approximation based on Neuber's hyperbola [12], Fig. 26, upper graph. The notched specimen used to determine design limits behaves similar under similar loading. Even if the loading of the specimen is kept in the elastic range, e. g. by dropping the pre-load history, the gained limits are known to yield reasonable results. So, elastically calculated stresses can be used as the driving force to describe fatigue at a notch. This is wide-spread practice.

The behavior of an EOC location under the same loading is different. As has been demonstrated, plastic yielding at the EOC is able to relevantly influence the stress amplitudes. An elastic calculation of the contact situation, referring to limits of notched specimens, does not contain any reflection of this peculiarity of contacting bodies. If the specimens to determine limits were designed to involve contact similar to the machine part, it may be expected that elastically calculated stresses of machine part and specimen are usable as the drivers for fatigue. This approach, however, is expensive.

Thus, when omitting costly contact specimen tests as provider of design limits it is advisable to apply plastic FEA in cases where yielding relevantly influences the behavior at the EOC. The latter is likely to occur in view of the drastic stress concentration typical at the EOC.

CONCLUSIONS

In view of the remaining geometrical change of bearing land pairing and change in tractions, both due to yielding, plasticity appears to be relevant in FEA simulations of recessive fixtures as applied in turbine blade design.

The plasticity-based material utilization $U_{\text{plast}} = 87\%$ (mean of Sines and Dang Van) appears closer to the target value of 100%, determined from EOC test, than the elastic model with $U_{\text{elast}} = 176\%$. The results of both criteria seem to be in good mutual accordance considering elastic and plastic FEA separately.

Part of the statements on utilization is the determination of design limits based on notched round specimens. They appear to provide applicable yet cost-effective results.

The relevance of plastic effects is further supported by the comparison of the elastically and plastically predicted fretting corrosion zone widths to measured widths. In contrast to the elastic calculation, the width gained with the plastic FEA is in the range of the measured results.

ACKNOWLEDGMENT

The authors acknowledge the financial support by the German Federal Ministry of Education and Research (BMBF) granted under project number 03FH071PX3. Responsibility for the contents of this publication lies with the authors.

REFERENCES

[1] Ambrico, J. M., and Begley, M. R., 2000. "Plasticity in fretting contact". *Journal of the Mechanics and Physics of Solids,* ***48***(11), pp. 2391–2417.

[2] Shin, K. S., 2009. "Prediction of fretting fatigue behavior under elastic-plastic conditions". *Journal of Mechanical Science and Technology,* ***23***(10), pp. 2714–2721.

[3] Sines, G., 1959. "Behavior of metals under complex static and alternating stresses". In *Metal Fatigue*, G. Sines and J. L. Waisman, eds. McGraw-Hill, New York, pp. 145–169.

[4] Dang Van, K., 1993. "Macro-micro approach in high-cycle multiaxial fatigue". In *Advances in Multiaxial Fatigue, ASTM STP 1191*, D. L. McDowell and R. Ellis, eds. American Society for Testing and Materials, Philadelphia, pp. 120–130.

[5] Charkaluk, E., Constantinescu, A., Maïtournam, H., and Dang Van, K., 2009. "Revisiting the Dang Van criterion". *Procedia Engineering,* ***1***(1), pp. 143–146.

[6] Dang Van, K., Griveau, B., and Message, O., 1989. "On a new multiaxial fatigue limit criterion: Theory and application". In *Biaxial and Multiaxial Fatigue, EGF 3*, M. W. Brown and K. J. Miller, eds. Mechanical Engineering Publications, London, pp. 479–496.

[7] Peridas, G., Korsunsky, A. M., and Hills, D. A., 2003. "The relationship between the Dang Van criterion and the traditional bulk fatigue criteria". *Journal of Strain Analysis for Engineering Design (Professional Engineering Publishing),* ***38***(3), pp. 201–206.

[8] ADINA R&D, INC., 2016. *ADINA Theory and Modeling Guide - Volume I: ADINA Solids & Structures, Release 9.2*. Watertown, MA.

[9] Mróz, Z., 1967. "On the description of anisotropic workhardening". *Journal of the Mechanics and Physics of Solids,* ***15***(3), pp. 163–175.

[10] Eaton, J. W., Bateman, D., Hauberg, S., and Wehbring, R., 2015. *GNU Octave version 4.0.0 manual: a high-level interactive language for numerical computations*. http://www.gnu.org/software/octave/doc/interpreter.

[11] Hoeppner, D. W., 2006. "Fretting fatigue case studies of engineering components". *Tribology International,* ***39***(10), pp. 1271–1276.

[12] Neuber, H., 2000. *Kerbspannungslehre: Theorie der Spannungskonzentration, Genaue Berechnung der Festigkeit*. Springer, Berlin.